ESTIMATING LOCAL AND NEAR-REGIONAL VELOCITY AND ATTENUATION STRUCTURE FROM SEISMIC NOISE

Peter Gerstoft[1], Jian Zhang[1], William A Kuperman[1], Nick Harmon[1], Karim G. Sabra[2], Michael C Fehler[3], Steven R Taylor[4]

University of California, San Diego[1], Georgia Institute of Technology[2], Massechusetts Institute of Technology[3], Rocky Mountain Geophysics, LLC[4]

Sponsored by Air Force Research Laboratory

Contract No. FA8718-07-C-0005[1–4]

ABSTRACT

This paper investigates the utility of computing Time-Domain Green's Functions (TDGF) to be used for estimating velocity and attenuation structure for the purposes of nuclear explosion monitoring over local and near-regional distances. Our objective is to extend and apply the methodology of deriving TDGF for propagation between two receivers by cross correlation of seismic noise and/or coda of earthquakes observed at the receivers and concentrates on the following four tasks:

1) The specific noise spectrum of the ocean microseism needs to be accounted for and compensated for in order to be able to measure group velocities across a wider bandwidth. The use of robust time-frequency analysis of the extracted coherent waveforms from seismic noise, provide a means to obtain broadband estimates of group velocities up to 0.5Hz for seismic stations located in coastal regions.

2) We are investigating methods to obtain spatial variations in attenuation using ambient noise. We assume that surface waves generated by atmospheric pressure fluctuations act as a forcing function on a damped harmonic oscillator system. The forcing function is adaptively updated from the network beam as a function of time. The relative attenuation at each site can be estimated from the width of the resonance peak relative to the driving forcing function.

3) Mean phase velocity dispersion curves are calculated for the TUCAN seismic array in Costa Rica and Nicaragua from ambient seismic noise using two independent methods, noise cross correlation and beamforming. The noise cross correlation and beamforming methods are compared and contrasted by evaluating results from the TUCAN array. The results of the two methods as applied to the TUCAN array agree within 1%, giving good confidence in the phase velocities extracted from noise.

4) From a data set recorded by a small-scale array (~4 km aperture), unbiased surface-wave Green's functions for short-periods less than 2 s have been extracted, as evidenced by a good match of noise-based impulse response with the borehole shot records sharing common paths. Beamforming has been used to identify specific directional noise, which may generate fast P-wave arrivals, thus needs to be analyzed with care. Such noise-based P-wave response and its reflections have turned out to be information-rich as well, revealing the lateral structure anomaly of the studied area.

OBJECTIVES

Our objective is to extend and apply the methodology of deriving time-domain Greens functions (TDGF) for propagation between two receivers by cross-correlation of seismic noise and/or coda of earthquakes observed at the receivers. We have previously shown that it is possible to obtain travel-time information for short-period surface waves (around 6 s) by cross-correlating seismic noise at local and regional scales. We propose to add the following improvements the TDGF method: 1) modifications to better handle cases having non-isotropic noise; 2) implementing a system identification approach for obtaining reliable amplitude information for the TDGF, allowing for the estimation of attenuation along paths between receivers, and 3) extracting TDGF from Lg or Sn coda.

RESEARCH ACCOMPLISHED

Improving surface-wave group-speed measurements using time-frequency analysis.

We have previously shown that estimates of the Time-Domain Green's Functions (TDGF) can be extracted from seismic noise cross-correlation (Sabra et al., 2005a, 2005b). This can to be used for measuring local velocity and attenuation structure for the purposes of nuclear explosion monitoring over local and near-regional distances. Using, 18 days of seismic noise recording in Southern California, we were able to obtain travel-time information for short period surface waves (around 7.5 s) by cross correlating seismic noise at local and regional scales. However, being able to measure broadband estimates of the Rayleigh wave group velocity can potentially provide a means to better constrain the inversion procedure about crustal velocity structure.

We have investigated signal-processing tools to improve the measurements of group-speed estimates from the cross-correlation waveforms. Surface waves are dispersive, and their associated dispersion curves can be used to invert for shear velocity profiles with depth. The main challenge with using surface waves, is the complexity of the required data processing and interpretation of the results. Our goal is to show robust time-frequency analysis of the extracted coherent waveforms from seismic noise improve the precision of group velocity measurements of surface waves. In particular, it is important to reduce the uncertainty of the dispersion curve measurements in order to minimize the number of acceptable earth models.

Group velocities are typically measured by computing spectrograms or the moving window method. In seismology they are often estimated using multiple filter banks. All these techniques result from Fourier transforms and thus create a large smearing in the time–frequency domain as a result of the Gabor-Heisenberg inequality (Gabor, 1946). An additional issue is the biases caused by the nonstationarity and the strongly varying spectral amplitude of the seismic signals. To mitigate those limitations, various time–frequency methods have been developed (Cohent, 1989). The Wigner-Ville transform $WV_{lm}(t,f)$ yields a time-frequency energy distribution of the cross-correlation $C_{lm}(t)$ (with analytic representation noted $\widetilde{C}_{lm}$ [Auger and Flandrin, 1995]) computed between two seismic noise recorded at sensors #l and #m:

$$WV_{lm}(t,f) = \int_0^T \widetilde{C}_{lm}(t+\tau/2)\widetilde{C}_{lm}^*(t-\tau/2)\exp(-i2\pi f\tau)d\tau \qquad (1)$$

We tested his approach on the cross-correlation waveform obtained from seismic noise recorded southwest of the Hawaiian Islands (Laske, 1999). 7 months of seismic noise (June 1997-Dec 1997) was recorded on a pair of OBS, 342km apart, and sampled at 25Hz. The seismic cross-correlation was computed following the methodology described in (Sabra et al. 2005a). We computed the Wigner Ville transform using the algorithm described in (Auger and Flandrin, 1995). In order to ease the visual interpretation of the signal's time-frequency structure, a smoothed version can be computed by a two-dimensional low-pass filtering of the Wigner-Ville transform in order to reduce the interference of cross-terms and noise artifacts (Fig. 1.a). Selecting the arrival-times along the maxima contours of the $WV_{lm}(t,f)$ yields an estimate of the change of the group velocity V_g vs. frequency f, of these coherent seismic waves between sensor pairs. As a complement to this smoothing, a reassigned representation of $WV_{lm}(t,f)$ is performed which essentially increases the concentration of the signal components (Fig. 1.b) (Auger and Flandrin, 1995), thus improving estimates of V_g. Extracting reliable and high resolution measurements of V_g are essential for the estimation of the earth velocity structure. Robust time-frequency analysis of the extracted coherent waveforms from seismic noise, appear to provide broadband estimates of group velocities up to at least 0.25Hz for seismic stations located in coastal regions.

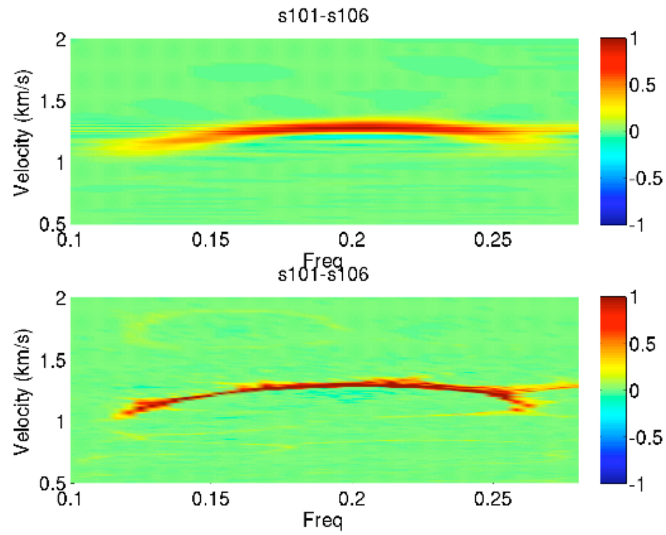

Figure 1 Time-frequency analysis of the extracted coherent between a pair of OBS located 343km apart southwest of the Hawaiian Islands, a) smoothed Wigner-Ville transform and b) Wigner-Ville transform after energy reassignment processing.

Extracting attenuation from noise

We have been using ambient seismic noise to construct attenuation maps beneath a network of stations. The approach we are looking at is to estimate the Q on a site-by-site basis as opposed to taking a tomographic approach (e.g. Matzel, 2008). The idea is to treat time-varying frequency-wavenumber (FK) beams of the ambient noise field as a forcing function beneath a network of stations. Each station responds differently to the forcing function depending on the site structure and attenuation. We use the differential equation for a forced, damped, harmonic oscillator to simulate the response of each station to the forcing function given by

$$\ddot{x}+\gamma\ddot{x}+\omega_0^2 x=\frac{1}{m}F(t) \tag{1}$$

where $F(t)$ is the forcing function, m is the mass, x is the sensor displacement response to the forcing function, γ is the viscous damping term and ω_0 is the natural frequency of the oscillator. The power spectrum of the sensor response (where m = 1) is given by

$$P_x(\omega)=\frac{P_F(\omega)}{\left[\left(\omega_0^2-\omega^2\right)^2+\left(\gamma\omega\right)^2\right]} \tag{2}$$

As will be further described below, we estimate the power spectrum of forcing function from the array beam on the maximum power of the ambient noise field. For light damping, $\gamma \ll \omega_0$, the power spectrum for a particular site relative to that of the forcing function is given by

$$P_{xF}(\omega)=\frac{P_x(\omega)}{P_F(\omega)}=\frac{1}{\omega_0^2\left[4\left(\omega_0^2-\omega^2\right)^2+\left(\dfrac{\omega}{Q}\right)^2\right]} \tag{3}$$

where $\gamma = \omega_0/Q$. For each station, it is then possible to grid search over a range of ω_0 and Q values to match the observed resonance peaks.

To find the power spectrum of the forcing function, $P_F(\omega)$, we first compute the time varying FK spectrum of the ambient noise impinging upon a network of stations. To test the methodology, we examined one day's worth of noise for a subset of 54 stations from the Southern California Seismic Network (SCSN). We computed the FK spectrum for two-hour window lengths an example of which is shown in Figure 2.

The noise predominantly arrives from the west and southwest for this particular time block. The black cross in Figure 2 shows the point having the maximum energy for the FK spectrum and we computed a beam from this point. In future work, we will examine the possibility of integrating a semi-circle of beams from the FK spectrum spanning a wider range of azimuths. In our preliminary study we have computed the beams from the maximum FK point for each of the two-hour time windows and computed the median power for the day as a power spectral estimate of the forcing function. Using the FK beam and the median power appears to eliminate the necessity of one-bit normalization commonly used to remove earthquakes from ambient noise time series.

Figure 3 shows the observed power spectral ratio, $P_{xF}(w)$, at a hard rock (CHF) and soft rock (BRE) site. Note that the resonance curve for the soft rock site is broader than that from the hard rock site indicating higher attenuation at the soft rock site. The solid line in Figure 3 shows the predicted resonance peak for a single oscillator frequency (Equation 4). The prediction appears to be too peaked suggesting that a more general absorption band model (e.g. Liu, 1976) may be necessary to fit the observed resonance peaks.

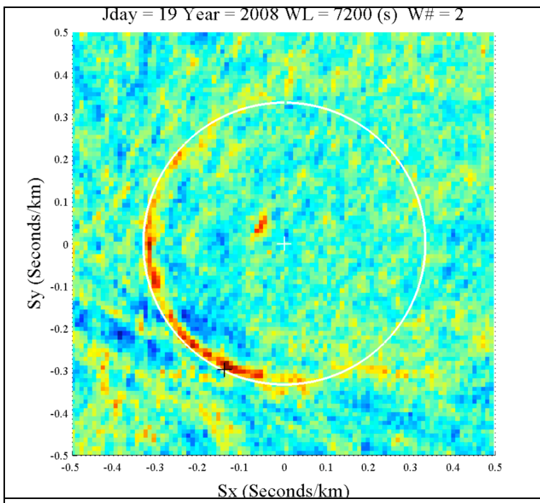

Figure 2. FK spectrum for a two-hour sample of ambient noise for a subset of 54 stations from the SCSN. White circle corresponds to a phase velocity of 3 km/s. Black cross indicates beam point.

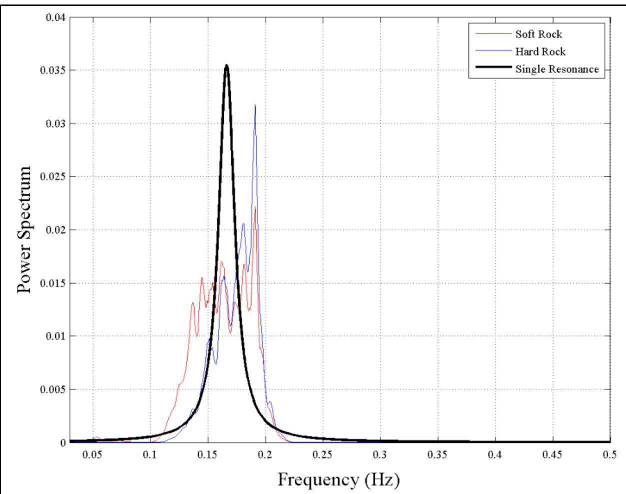

Figure 3. Power spectral ratio, $P_{xF}(w)$, observed at a hard rock and soft rock site. Black line is prediction of power spectral ratio for a single resonance peak (Equation 3).

Midscale seismic beamforming and Noise crosscorrelation

We determined phase velocities using 593 days (July 2004 to March 2006) of station to station NCF for the vertical components of the 49 stations of the TUCAN seismic array (Figure 4c) using a method similar to *Harmon et al*. (2007). Variations from *Harmon et al*. (2007) include removing the instrument responses from the signals (the TUCAN contains different sensor types), decimation to 1 s sampling, a RMS clipping scheme for the daily time series (Sabra et al., 2005) and signal whitening by normalizing the Fourier coefficients by their respective magnitude, both to create a single broadband NCF. Then we cross correlated hourly time series segments for all station pairs and stacked the resulting correlograms. The NCF phase dispersion was determined by unwrapping the phase of the stacked NCF and applying a $\pi/4$ correction. We determined the cycle ambiguity by matching the average phase velocity determined from teleseismic events at 20 s period (Abers el al., 2007). The mean teleseismic phase velocity estimates were determined using the method of Yang and Forsyth (2006), with 95 events with good azimuthal coverage.

We calculate the mean phase dispersion curve and its standard error of the mean by station-to-station distance-weighted averaging. A station-to-station NCF phase velocity estimate was used to calculate the mean phase dispersion curve if 1) the NCF had signal to noise ratio >10, 2) the temporal average of ~4 month NCF stacks had a standard deviation of < .1 km/s and 3) the station-to-station path was greater than 3λ after Lin et al. (2008), Distance weighting was chosen since longer paths should be more representative of average structure. For 15-29 s periods, the teleseismic and NCF mean phase velocity estimates were within 1%, except at 18 s where they were within 2%.

For station-to-station paths perpendicular to the Pacific coast, the NCFs are dominated by 6-10 s microseisms coming from the coast. This can be seen by comparing NCFs with comparable path lengths and different orientations such as N1–N13 and B4–N11 (Figure 4f,e). A high frequency signal owing to the Pacific microseisms is seen at negative lag (from southwest) for the path perpendicular to the Pacific coast whereas no high frequency signal is seen at positive lag for this path (Figure 4f) or for positive and negative lags of the coast parallel paths (Figure 4d,e). The amplitudes and frequency contents of the NCFs suggest that the noise distribution changes with period.

For periods between 10-22 s, the Beamformer output in Figure 5 there is a nearly continuous ring maximum with surface wave slownesses, suggesting surface waves dominate the signal in this period range, which is consistent with the 2D model of noise distribution. Above 18 s period there is little signal from the Pacific (180-240°), while in the secondary microseism band (6-10 s period) the dominant source direction is 180-240° azimuth with little energy coming from other directions, which is consistent with what was observed in the NCF.

For periods greater than 6 s, both NCF and beamformer average phase velocity estimates are within error of each other (Figure 6). For the best-resolved periods (7-20 s), the phase velocity from beamforming agrees within 1% with the NCF estimates. The agreement is best in this band because this is where the microseisms are strongest (see Figure 5). Below 6 s period, the agreement between the two estimates begins to erode due to aliasing as the beamformer output no longer resolves any coherent surface waves and the errors in the NCF estimates increase. The NCF estimate is more stable due to the inherent averaging in the frequency domain caused by windowing in the time domain. The station geometry requirements for the two methods are different. The NCF method requires only 2 stations. Beamforming, on the other hand, requires an array of stations. We choose NCF station spacing to be at least 3λ at 20 s period to avoid near field effects and to allow distinct phases to emerge (*Bensen et al,* 2007). Data selection requirements of the NCF limit the number of station pairs to 270 out of 1149 at 20 s. For beamforming array aperture larger than 1λ is required to resolve the longest periods of interest and station spacing < λ/2 to prevent spatial aliasing at shortest periods for a regularly spaced array, but for irregular arrays it can be relaxed somewhat. For the TUCAN array which consists mainly of two regularly-spaced line arrays pointing southwest, beamforming aliasing manifests itself as a straight-line beamformer output (perpendicular to the line array directions) rather than a point for sources coming from the southwest, as shown in the 7 s band in Figure 5. For shorter periods, the beamformer aliasing becomes more severe making it difficult to extract phase velocities. In the 7-20 s bands, the phase slowness can be resolved but aliasing does contribute to the errors in the phase slowness estimates. Overall, the aliasing at the periods of interest, 7-20 s, is minor while it dominates at periods less than 7 s.

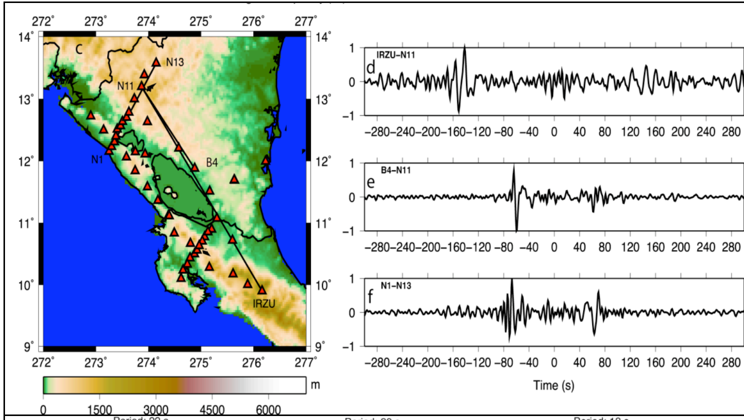

Figure 4. Station locations (red triangles) and topography (from ETOPO2) of the TUCAN array. The time series show the normalized bandpass filtered (5-33 s) NCF between station (d) IRZU-N11, (e) B4-N11, and (f) N1-N13. Positive lags correspond to waves traveling from N11 and N13.

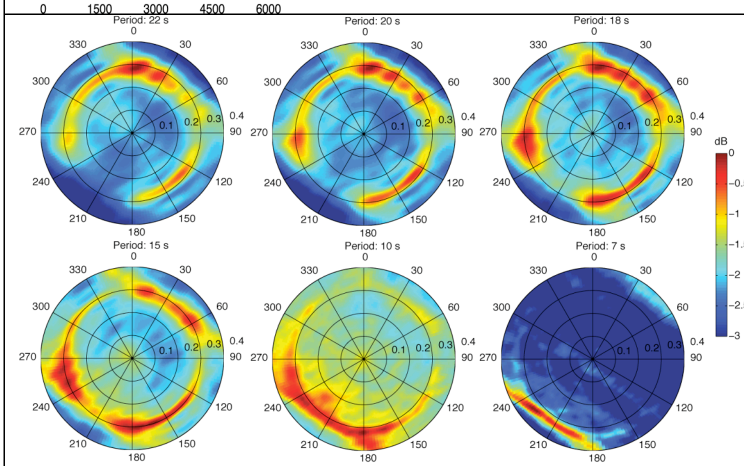

Figure 5. Azimuth vs. phase slowness plots of 593-day stack of beamformer output (dB) of the TUCAN array for 7, 10, 15, 18, 20 and 22 s period. Slowness is the radial distance on the polar plots from 0.00-0.4 s/km.

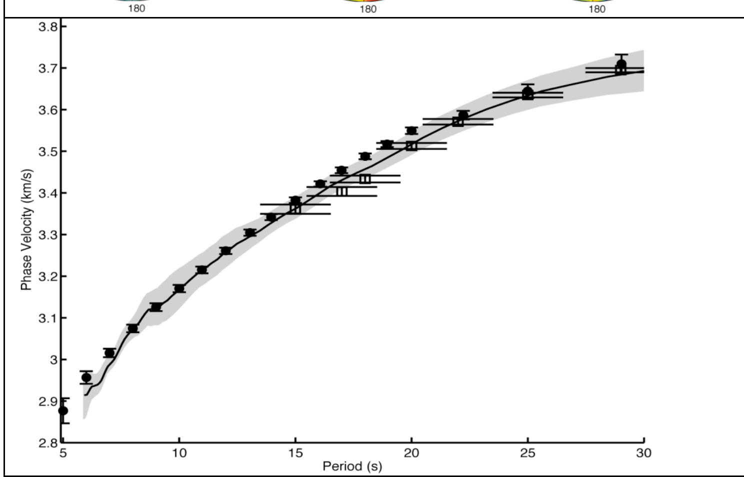

Figure 6. Phase velocity estimates from beamforming (solid black line) with 3x standard error of the mean (grey region), noise correlation methods (circles) with 3x standard error of the mean bars and teleseismic phase velocity estimates (open squares) with 3x standard error of the mean.

Local-scale seismic noise cross-correlation (NCC) from the Calico fault experiment

In this work we present the seismic noise cross-correlation (NCC) results from a data set recorded by a dense array (~ 5 km aperture, see Figure 7a) along the Calico fault in California's Mojave desert. The data set is unique for NCC study in terms of: (1) local scale (a few km); (2) long recordings (~ 6 months); and (3) common site of a sensor and a borehole shot, allowing direct comparison of the noise-based Green's functions with the shot records. Our goal is to demonstrate the successful retrieval of reliable Green's functions from a noise field with a strong P-wave component, and the application of seismic NCC for revealing fault zone structures.

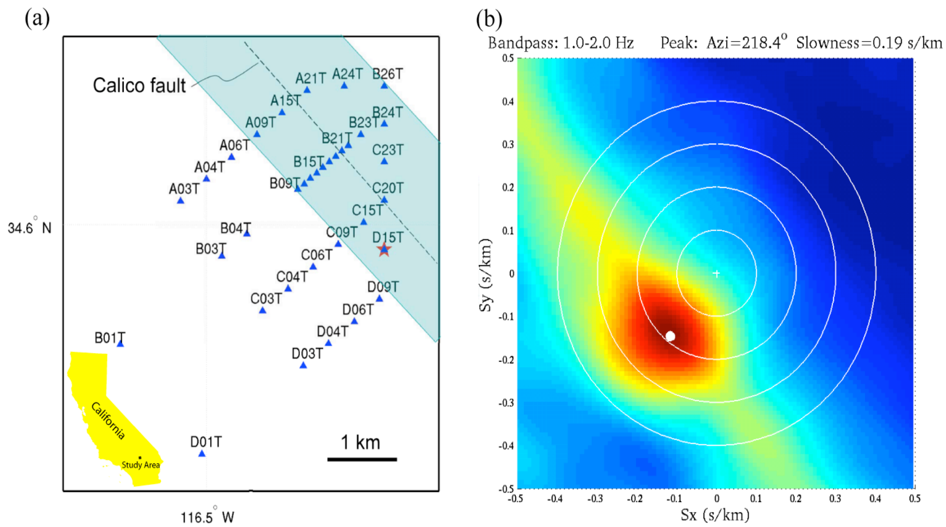

Figure 7. (a) Map of the Calico fault area, showing stations (blue triangles), a borehole shot (red star), the Calico fault trace (dashed), and the fault zone (light blue); (b) Slowness-azimuth distribution of the noise field from beamforming, stacked over frequency band of 1-2 Hz.

Over broad band, the major part of the noise in southern California are microseisms mainly coming from the Pacific ocean (e.g., Gerstoft and Tanimoto, 2007). Here we focus on the frequency band of 0.5-3.0 Hz, in which microseisms may not be predominant. Using vertical-component noise records, we show in Figure 7b a one-day beamforming output stacked over 1.0-2.0 Hz. Clearly the noise field is dominated by a coherent energy coming from SW, at an apparent speed of ~ 5 km/s. Such slowness-azimuth pattern holds for all the other days within the 6 months period, indicating that this incident energy is temporally and spatially stable. Given the apparent speed of ~ 5 km, it is too fast to be a surface wave. We further suggest that it is a P wave as it is strongest on the vertical component.

From beamforming results, apparently a plane wave arrives at the array from the lower crust or upper mantle. We then expect to see a peak in the NCC output of a pair of sensors, of which the time lag from zero corresponds to the effective inter-receiver distance along the direction of incident wave, rather than the one along the surface. The time when the peak emerges would be a *cosine* function of the difference between the azimuths of the station-pair axis and the incident wave. Note, that for the case of abody-wave, such a peak is no longer related to neither surface-wave nor body-wave Green's function. However, we still expect to see surface-wave Green's functions in the NCC outputs, as long as a diffusive wavefield (at least partially) coexists.

Indeed we observe both a fast and a slow wave packet in the NCC output of each pair. Both appear propagating from the record-section (not shown) of the NCC traces having directions roughly along NE-SW. The fast wave packet has a speed of about 5 km/s (getting faster for station pairs with azimuths away from NE-SW, e.g., arriving at zero along NW-SE), confirming that it is originated from the ballistic body wave observed from beamforming. The slow one turns out to be a packet of surface-wave Green's functions, as verified by a good match, for a range of distance and azimuth respectively, of the noise-based impulse responses (the derivative of NCC outputs) with the records of a borehole shot sharing common paths (Figure 8). This comparison is a particular advantage of our experiment as we deployed a sensor (D15T in Figure 7a) at essentially the same site as the shot (red star in Figure 7a).

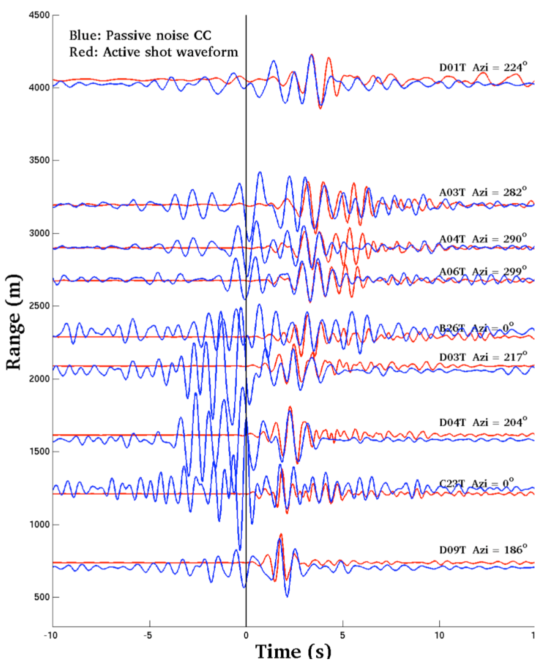

Figure 8. A good match of noise-based Surface-wave Green's functions (blue) with the borehole shot records sharing common paths.

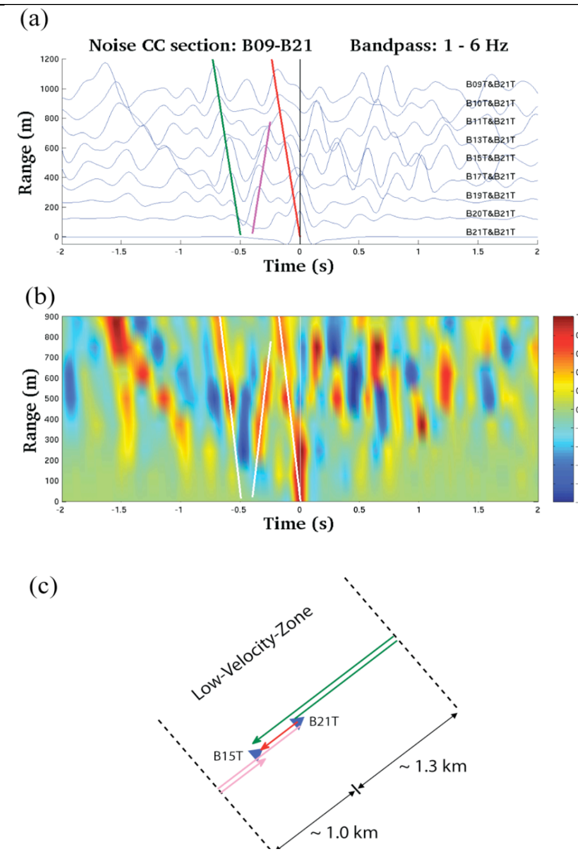

Figure 9. (a) Record-section of the NCC, for the profile B09T-B21T. Lines of red, purple, and green mark the direct arrival and its reflections from the side walls of LVZ, respectively. (b) Same as in (a), except the amplitude of the signals shown in color scale. (c) A LVZ model showing an example of the corresponding virtual arrivals from B21T to B15T.

Our results indicate that the NCC technique is feasible and robust in converging Green's functions even for the noise field dominated by strong ballistic waves. However, caution is needed to distinguish body-wave Green's functions from plane-wave generated impulse responses. Although the case we provided is for near-field, i.e., scales less than a few wavelengths, which means that specific modes of surface waves are not well developed yet, Green's functions emerged from noise may still find their applications in exploration, engineering, and explosion monitoring fields, e.g. surface-wave isolation/removal.

The P-wave noise identified in our experiment provides a stable natural source for studying the structures along the Calico fault. By performing NCC for pairs of sensors along a profile (B09T-B21T, see Figure 7a), we construct a virtual record-section (Figure 9a) as if a plane-wave source with an apparent speed of 5 km/s were placed at the site of B21T. Interestingly as seen in Figure 9a and 9b, besides the direct arrival of the virtual event (marked by a red line), another two arrivals with the same absolute speed show up (marked by a purple line and a green line respectively). Indeed, these three arrivals can be interpreted by a low-velocity-zone (LVZ) model shown in Figure 9c. Thus the wave from a virtual source at B21T will be reflected back from both sides of the boundaries of LVZ. From the direct arrival and its reflections in the record-section, our inversion of the distance from B21T to the reflectors (i.e., side walls of LVZ) amounts to 1.0 km and 1.3 km, respectively. Thus we estimate that the width of the Calico fault LVZ is about 2.3 km, which agrees favorably with other evidences (Radiguet, unpublished material).

CONCLUSIONS AND RECOMMENDATIONS

1) Using time-frequency anysis methods more robust estimates of the surface wave group velocity can be obtained.

2) Seismic attenuation near a station can be extracted from noise by assuming the ambient noise obtained from a time-variable FK beam acts as a forcing function on a damped harmonic oscillator system.

3) Beamformer output provides valuable information about noise distribution through time. We show that from 7-20 s period seismic noise in clipped seismograms for 18 months of data is dominated by surface waves and is consistent with a 2D model of noise distribution, having good azimuthal coverage from 10-22 s period. Beamforming provides an accurate, independent estimate of the mean phase velocity dispersion across a seismic array that is within 1% of NCF and teleseismic estimates. Thus, beamforming can potentially resolve the cycle ambiguity in NCF phase velocity estimates without a complimentary teleseismic study.

4) We provide results of a local-scale (~ 5km x 5km) seismic NCC experiment at frequency band of 0.5 Hz and above. By applying beamforming, we identify a strong P wave in the noise field, suggesting that a careful analysis of the noise distribution and wave type is needed in the efforts of extracting P-wave Green's functions. By comparing the noise-based surface-wave Green's functions with the borehole shot records sharing common paths, we obtain a good match and thus verify the robustness of the NCC technique for a noise field dominated by a body wave. We then find that the NCC can turn the ballistic P-wave noise into a virtual record-section of a profile of sensors. From the direct arrival and its reflections shown in the record-section, we invert the width of the Calico fault LVZ to be ~ 2.3 km.

REFERENCES

Abers, G. A., K. M. Fischer, M. Protti, and W. Strauch (2007), The TUCAN Broadband Seismometer Experiment: Probing Mantle Melting in the Nicaragua-Costa Rica Subduction Zone, *IRIS Newsletter*(1), 10-12.

Auger, A., Flandrin, P. (1995). "Improving the readability of time-frequency and time-scale representations by the reassignment method". IEEE Trans. Sig. Process*,* 43, 1068-1089.

Bensen, G. D., M. H. Ritzwoller, M. P. Barmin, A. L. Levshin, F. Lin, M. P. Moschetti, N. M. Shapiro, and Y. Yang (2007), Processing seismic ambient noise data to obtain reliable broad-band surface wave dispersion measurements, *Geophys. J. Int.*, *169*, doi: 10.1111/j.1365-1246X.2007.03374.x.

Cohen, L., (1989), "Time-frequency distribution—A review", Proc. IEEE, 77, No. 7, 941–981.

Gabor, D., (1946), "Theory of communication", J. Inst. Electron. Eng., 93, 429–457.

Gerstoft, P., and T. Tanimoto (2007), A year of microseisms in southern California, *Geophys. Res. Lett.*, *34*, L20304, doi:20310.21029/22007GL031091.

Harmon, N., D. Forsyth, and S. Webb (2007), Using Ambient Seismic Noise to Determine Short-Period Phase Velocities and Shallow Shear Velocities in Young Oceanic Lithosphere *Bull. Seis. Soc. Am.*, *97*, 2024-2039.

Laske, G., Phipps Morgan, J., and Orcutt, J.A., (1999), First results from the Hawaiian SWELL pilot experiment: Geophysical Research Letters, v. 26, p. 3397–3400, doi: 10.1029/1999GL005401.

Lin, F., M. P. Moschetti, and M. H. Ritzwoller (2008), Surface wave tomography of the western United States from ambient seismic noise: Rayleigh and Love wave phase velocity maps, *Geophys. J. Int.*, doi:10.1111/j1365-1246X.2008.03720.x.

Liu, H.P., D.L. Anderson and H. Kanamori, Velocity dispersion due to anelasticity: Implications for seismology and mantle composition, *Geophys. J.R. Astron. Soc.*, 47, 41-58, 1976.

Matzel, E.M., Attenuation tomography using ambient noise correlation, *Seism. Res. Lett.,* 79, 358, 2008.

Sabra, K., P. Gerstoft, P. Roux, W. A. Kuperman, M. Fehler (2005a), "Extracting time-domain Green's Function estimates from ambient seismic noise," Geophysical Research Letters, 32.

Sabra, K., P. Gerstoft, P Roux, W.A. Kuperman, M. Fehler (2005b). Surface wave tomography from microseisms in Southern California, AGU *Geophys. Res. Lett*. 32: L14311, doi:10.1029/2005GL023155.

Yang, Y., and D. W. Forsyth (2006), Regional tomographic inversion of amplitude and phase of Rayleigh waves with 2-D sensitivity kernels, *Geophys. J. Int.*, *166*(3), 1148-1160.